# Chloride facilitates Mn(III) formation during photo-assembly of the Photosystem II oxygen-evolving complex

Brandon P. Russell and David J. Vinyard*

Department of Biological Sciences
Louisiana State University
Baton Rouge, LA 70803, USA

*Corresponding author: dvinyard@lsu.edu

ORCID: D.J.V. 0000-0002-8058-5998
B.P.R. 0000-0003-1382-9945

## Abstract

The $Mn_4Ca$ oxygen-evolving complex (OEC) in Photosystem II (PSII) is assembled in situ from free $Mn^{2+}$, $Ca^{2+}$, and water. In an early light-driven step, $Mn^{2+}$ in a protein high-affinity site is oxidized to $Mn^{3+}$. Using dual-mode electron paramagnetic resonance spectroscopy, we observed that $Mn^{3+}$ accumulation increases as chloride concentration increases in spinach PSII membranes depleted of all extrinsic subunits. At physiologically relevant pH values, this effect requires the presence of calcium. When combined with pH studies, we conclude that the first $Mn^{2+}$ oxidation event in OEC assembly requires a deprotonation that is facilitated by chloride.

## Keywords

Photosystem II, oxygen-evolving complex, assembly, electron paramagnetic resonance spectroscopy

## Introduction

Water oxidation in Photosystem II (PSII) occurs at a $Mn_4Ca$ cluster known as the oxygen-evolving complex (Shen 2015, Vinyard and Brudvig 2017). This active site is assembled in situ without the use of chaperones. During the photo-assembly process, $Mn^{2+}$ is oxidized to $Mn^{3+}$ or $Mn^{4+}$ and water molecules are deprotonated to form μ-oxo or μ-hydroxo bridging ligands (Dasgupta et al. 2008, Bao and Burnap 2016).

As illustrated in Figure 1, OEC photo-assembly begins with $Mn^{2+}$ binding to a "high-affinity site" with an equilibrium $K_d$ of approximately 40 μM (Tyryshkin et al. 2006). $Ca^{2+}$ is either already present near the high-affinity site or binds subsequently to $Mn^{2+}$ (Miller and Brudvig 1989, Chen et al. 1995). As first described by Radmer and Cheniae (1971), the first oxidation event (Figure 1, A to B) is light dependent and highly reversible. The conversion of B to C does not require light and represents the rate-limiting step of photo-assembly. Once C is formed, it is oxidized in a light-dependent process to D, which rapidly and efficiently is assembled into a functional OEC.

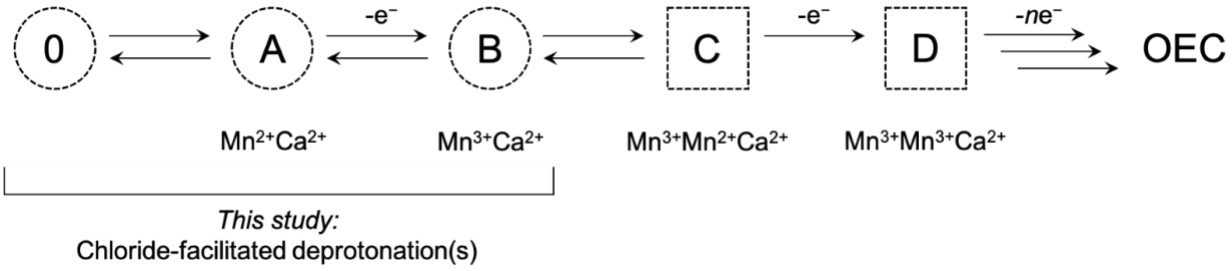


**Figure 1.** Current model of OEC photo-assembly. The vacant high-affinity site, intermediate 0, is occupied by $Mn^{2+}$ and likely $Ca^{2+}$ to form intermediate A. Light-induced oxidation results in the formation of transient intermediate B. Following a slow light-independent event (represented by conversion of circles to squares), C is formed, and the remaining steps occur rapidly. This study examines the events leading to the formation of intermediate B.

Recently, we used kinetics and photo-assembly yields to show that equilibrium-controlled steps leading to the formation of intermediate C display an inverse H/D isotope effect that is chloride dependent. We interpreted our results to suggest that these processes involve one or more deprotonation events that are facilitated by chloride (Vinyard et al. 2019). In this model, chloride serves a similar function in OEC photo-assembly as it does during OEC catalytic turnover (Pokhrel et al. 2011).

Here, we refine and extend this model using data from electron paramagnetic resonance (EPR) spectroscopy. Intermediate B contains one $Mn^{3+}$ center ($S = 2$) that can be observed using parallel polarization EPR (Campbell et al. 2000). In PSII samples from plants, Dismukes and coworkers observed that the yield of intermediate B induced by low-temperature illumination increases with increasing pH (Tyryshkin et al. 2006, Dasgupta et al. 2009). This result is surprising given the acidic nature of the thylakoid lumen. Here, we show that the addition of chloride and calcium facilitates $Mn^{3+}$ formation at physiologically relevant pH values. The likely mechanism involves a

deprotonation event of a primary Mn ligand that makes the $Mn^{3+}/Mn^{2+}$ reduction potential more favorable.

## Methods

Apo-OEC-PSII membranes were prepared using identical methods as previously reported (Vinyard et al. 2019). These $CaCl_2$ and hydroxylamine treated preparations are fully depleted of manganese and the extrinsic subunits PsbO, PsbP, and PsbQ.

For photo-assembly experiments, apo-OEC-PSII membranes were washed twice then resuspended at 7 mg Chl $mL^{-1}$ in a buffer containing 20 mM MES-NaOH, pH 6.0, 20 mM NaCl, 8 mM $NaHCO_3$, 40 mM $CaCl_2$, 160 µM $MnCl_2$, 400 mM sucrose, and 10 µM dichlorophenolindophenol. We did not vary bicarbonate concentration in this study and chose to use a constant concentration of 8 mM to ensure that the non-heme iron on the acceptor side of PSII had the correct ligand environment (Brinkert et al. 2016). Aliquots for each EPR sample were spun down and resuspended in the same buffer. Stock solutions containing 5 M NaCl and 500 mM MES-NaOH at pH 5.5, 6.0, 6.5, and 7.0 were added to vary $[Cl^-]$ and pH. The final chlorophyll concentration was 5 mg $mL^{-1}$. Final pH values were measured as 5.6, 6.0, 6.3, and 6.6, respectively. Samples were loaded into quartz EPR tubes, purged with argon, sealed, and frozen in liquid nitrogen.

For calcium-depleted samples, aliquots were washed twice with the buffer above except $CaCl_2$ was omitted and NaCl was increased to 100 mM. The samples were then resuspended in this buffer and total chloride was adjusted using a 5 M NaCl stock solution if necessary. The final chlorophyll concentration was 5 mg $mL^{-1}$.

EPR spectra were measured at X-band using a Bruker EMX spectrometer equipped with an ER4116DM dual mode resonator and an Oxford ESR-900 helium flow cryostat. Temperature was maintained at 5.0 ± 0.1 K for all experiments. For $Mn^{2+}$ detection in perpendicular mode, experimental parameters were microwave frequency, 9.63 GHz; modulation frequency, 100 kHz; modulation amplitude, 9.8 G; sweep time, 60 s; conversion time, 65 ms; time constant, 164 ms; microwave power, 5 µW. For $Mn^{3+}$ detection in parallel mode, experimental parameters were microwave frequency, 9.37 GHz; modulation frequency, 100 kHz; modulation amplitude, 9.8 G; sweep time, 60 s; conversion time, 109 ms; time constant, 164 ms; microwave power, 25 mW.

For each sample, an initial perpendicular mode scan in darkness was acquired. Samples were then transferred to a 90% ethylene glycol, 10% ethanol, dry ice bath maintained at -20°C (Jensen and Lee 2000) and illuminated for 30 minutes with a red LED ($\lambda_{max}$ = 623 nm, 4-5 W optical power, ThorLabs). EPR tubes were first transferred to liquid nitrogen then the EPR cryostat. Both perpendicular and parallel mode scans were performed on each illuminated sample.

Relative $Mn^{3+}$ concentrations were determined by the peak-to-trough height of the fourth hyperfine feature (around 850 G, (Tao et al. 2018)). Simulations were performed using EasySpin 5.2 (Stoll and Schweiger 2006).

Data represent the average of two biological replicates and were normalized to the highest observed signal.

## Results

Based on methods developed by Miller and Brudvig (1990) and previously utilized by the groups of Britt (Campbell et al. 2000) and Dismukes (Tyryshkin et al. 2006, Dasgupta et al. 2009), $Mn^{2+}$ is oxidized in apo-OEC-PSII samples when illuminated at moderately low temperatures such as -20°C. As illustrated in Figure 2, the intensity of the six-line $Mn^{2+}$ EPR spectrum using perpendicular polarization decreases following illumination. For these extrinsics-depleted PSII membrane samples, 100 mM chloride (Figure 2A) is sub-saturating for optimal photo-assembly rates and yields while 500 mM chloride (Figure 2B) is saturating (Miyao and Inoue 1991, Vinyard et al. 2019).

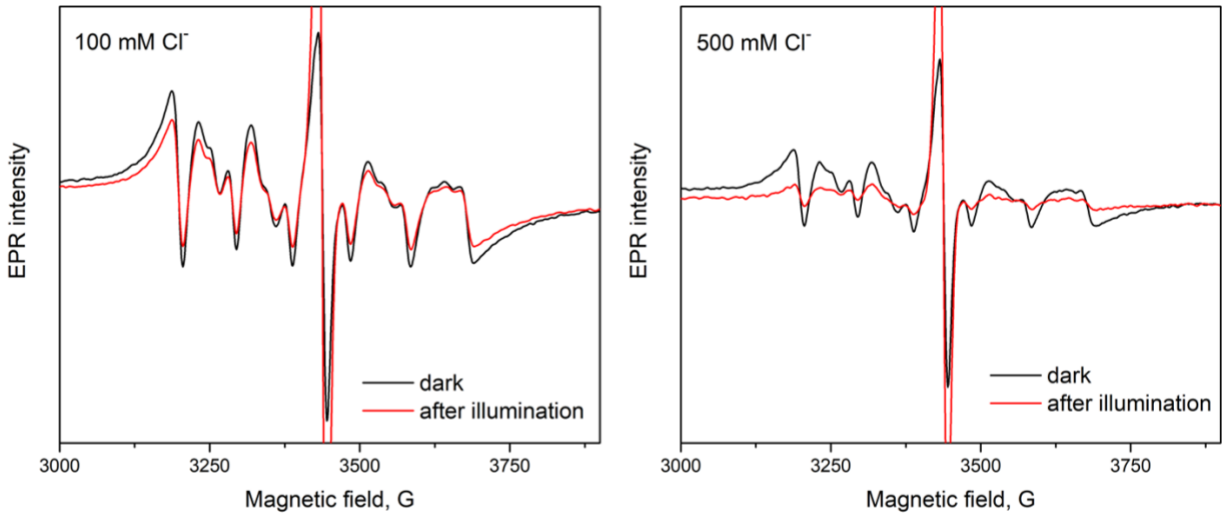


**Figure 2.** $Mn^{2+}$ EPR spectra using perpendicular polarization before (black) and after (red) illumination at -20°C. Samples were prepared with 25 μM apo-OEC-PSII and 160 μM $Mn^{2+}$ at pH 6.0 with either 100 mM total chloride (left) or 500 mM total chloride (right). Both samples contained 40 mM $Ca^{2+}$. EPR parameters are described in Methods.

As further illustrated by the complete set of spectra in Figure S1, both pH and chloride concentration affect the quantity of free symmetric $Mn^{2+}$ in the dark that contributes to the six-line signal. Qualitatively, the decrease in the $Mn^{2+}$ EPR signal after illumination is greater at higher pH values and higher chloride concentrations.

While the need for high chloride concentrations and high pH is consistent with earlier work, the latter condition is at odds with the thylakoid lumen environment where photo-assembly occurs (pH 5.8 – 6.5, (Kramer et al. 1999)) and motivated further analysis.

Using parallel polarization, a six-line signal centered at $g$ = 8.1 is observed after illumination at moderately low temperatures (-20°C) as previously shown (Figure 3) (Campbell et al. 2000, Tyryshkin et al. 2006, Dasgupta et al. 2009). This feature is an axial component of a broad EPR spectrum centered at $g$ = 2 (Campbell et al. 2000). At the physiologically relevant pH value of 6.0, we observed that the intensity of the six-line feature increased as chloride concentration increased (Figure 3, upper panel).

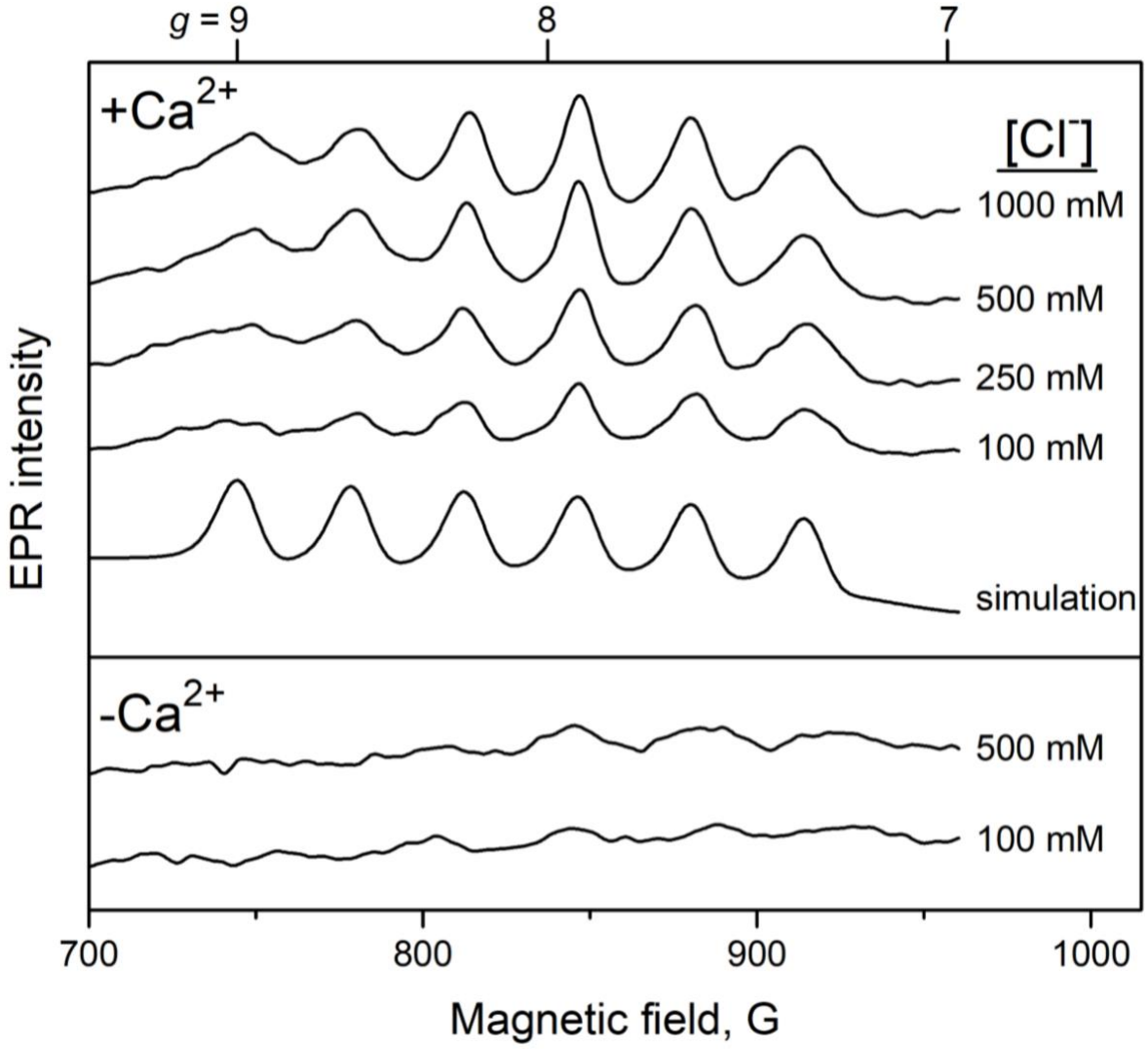


**Figure 3.** $Mn^{3+}$ EPR spectra using parallel polarization after illumination at -20°C. In the upper panel, chloride concentration was varied from 100-1000 mM at pH 6.0 in samples containing 40 mM $Ca^{2+}$. Simulation parameters are described in the text. In the lower panel, $Ca^{2+}$ was omitted from the sample buffer. EPR parameters are described in Methods.

The observed $Mn^{3+}$ parallel polarization spectrum was simulated using parameters similar to previous reports (Campbell et al. 2000, Tyryshkin et al. 2006, Dasgupta et al. 2009). The simulation in the upper panel of Figure 3 used $A_{//}$ = 33.5 G, D = -2.4 $cm^{-1}$, E/D = 0.092, and line broadening with HStrain (Stoll and Schweiger

2006). No change in hyperfine magnitude was observed between the samples analyzed.

To expand upon the data shown above, we prepared samples at pH values of 5.6, 6.0, 6.3, and 6.6, with total chloride concentrations of 100, 250, 500 and 1000 mM. Two biological replicates were analyzed. A heat map representing the averaged and normalized $Mn^{3+}$ parallel polarization EPR signal intensity is shown in Figure 4 and complete data are shown in Figure S2. More $Mn^{3+}$ is accumulated following illumination at higher pH values and higher chloride concentrations. This result is qualitatively consistent with the $Mn^{2+}$ data in Figure S1.

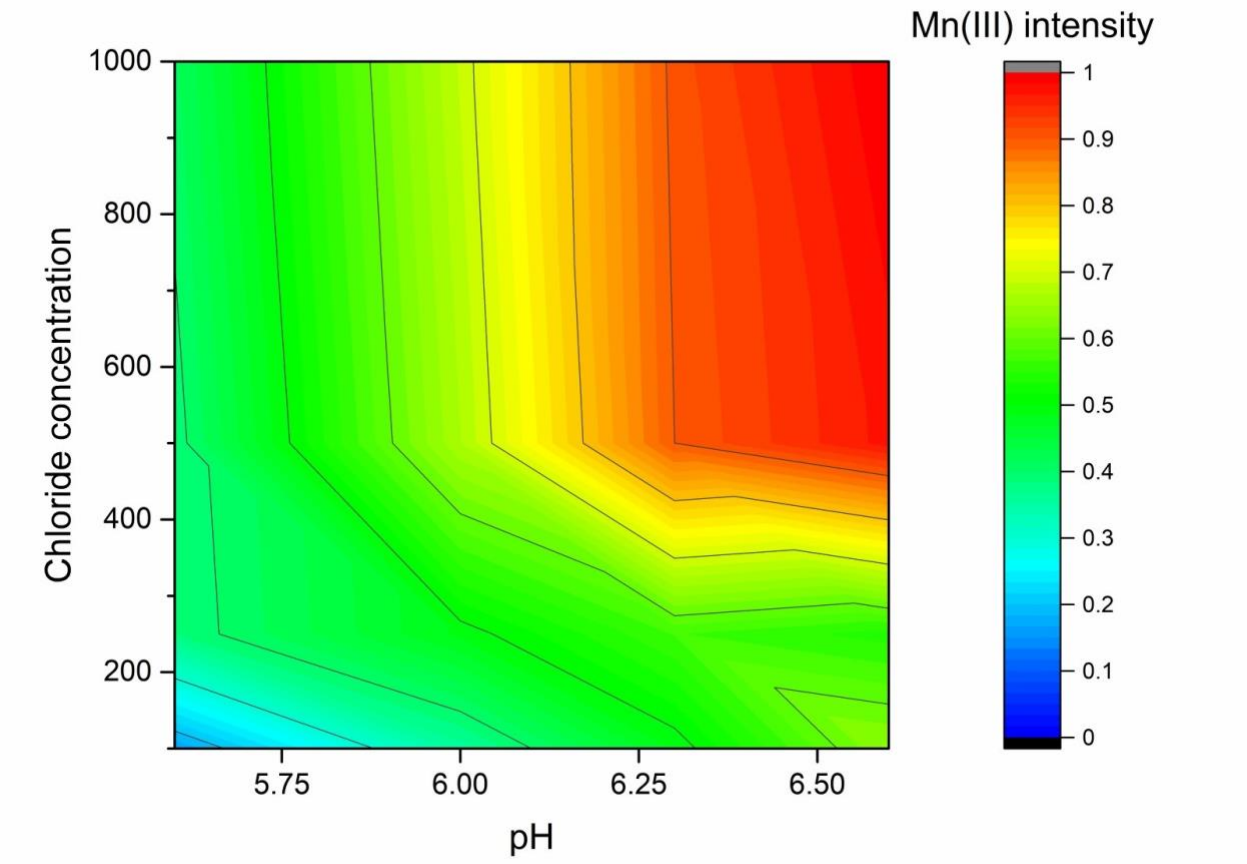


**Figure 4.** $Mn^{3+}$ parallel polarization EPR signal intensity as a function of chloride concentration and pH. The heat map was generated from 16 data points with pH values of 5.6, 6.0, 6.3, and 6.6, and chloride concentrations of 100, 250, 500 and 1000 mM.

Prior work has implicated a role for calcium in the formation of intermediate B in OEC photo-assembly (Tyryshkin et al. 2006). To test whether calcium was a factor in the observed chloride effect, calcium was omitted and NaCl was added to samples at pH 6.0 at sub-saturating (100 mM) and saturating (500 mM) chloride concentrations. As shown in the lower panel of Figure 3, the $Mn^{3+}$ parallel polarization EPR signal was not observed above the noise level at either chloride concentration when calcium was removed from the sample buffer.

## Discussion

To assemble a PSII OEC active site, $Mn^{2+}$ must first bind to the protein matrix (0 to A in Figure 1). This association is fairly weak with an equilibrium (dark) $K_d$ of 40-50 µM. Once $Mn^{2+}$ is bound and light is provided, $Mn^{2+}$ is oxidized with a low quantum yield (A to B in Figure 1). In the slowest step of photo-assembly, something happens independent of light to stabilize the resulting $Mn^{3+}$ intermediate (B to C in Figure 1). The remaining steps (C to a functional OEC) are first order with respect to C. Determining the mechanisms of the early photo-assembly steps that lead to intermediate C is critical for understanding this overall process and motivated the current work.

We previously showed that chloride facilitates one or more deprotonation events in OEC photo-assembly (Vinyard et al. 2019). Those results indicate that chloride increases the yield of the overall process by increasing the equilibrium concentration of intermediate C and that chloride increases the rate of the rate-determining step (presumably B to C). Here, we show that chloride is specifically involved in the accumulation of the first $Mn^{3+}$ intermediate (B). Interestingly, this reaction requires calcium and is favored at higher pH values.

The spinach PSII membrane samples used here were fully depleted of all extrinsic subunits, including PsbO. This treatment facilitates OEC photo-assembly by providing a more open protein conformation (Burnap et al. 1996, Roose and Pakrasi 2008, Avramov et al. 2020) but dramatically decreases the binding affinity of chloride (Miyao and Inoue 1991, Vinyard et al. 2019). Earlier work on spinach PSII membranes showed very little observable $Mn^{3+}$ formation (Tyryshkin et al. 2006, Dasgupta et al. 2009) at the physiologically relevant pH range of 5.8-6.5 (Kramer et al. 1999).

In this study, $Mn^{2+}$ was added to apo-OEC-PSII samples at 0-4°C in darkness during which time intermediate 0 was partially converted to intermediate A. To form intermediate B, the samples were frozen then illuminated at -20°C where little diffusion is expected. The chloride effect observed here may influence the interrelated processes of $Mn^{2+}$ binding affinity, proton release before formation of B, and the reduction potential of $Mn^{2+}$ oxidation to $Mn^{3+}$.

A recent cryo-EM study of a cyanobacterial apo-OEC-PSII intermediate observed an ion in a binding site comprised of D1 residues D170, E189, and H332 (Figure 5 (Zabret et al. 2021)). A similar binding site for $Mn^{2+}$ was determined independently through QM/MM and FTIR studies (Sato et al. 2021) starting with an earlier apo-OEC PSII structure (Gisriel et al. 2020). In both cases, D1-H332 likely interacts with the ion through a bridging water molecule. An ion in this site is 4.5 Å from $Y_Z$ (Zabret et al. 2021), which is very similar to the position of $Ca^{2+}$ in the fully assembled OEC (4.7 Å from $Y_Z$ (Umena et al. 2011)). Chloride binds to a distal position between D1-H332 and D2-K317.

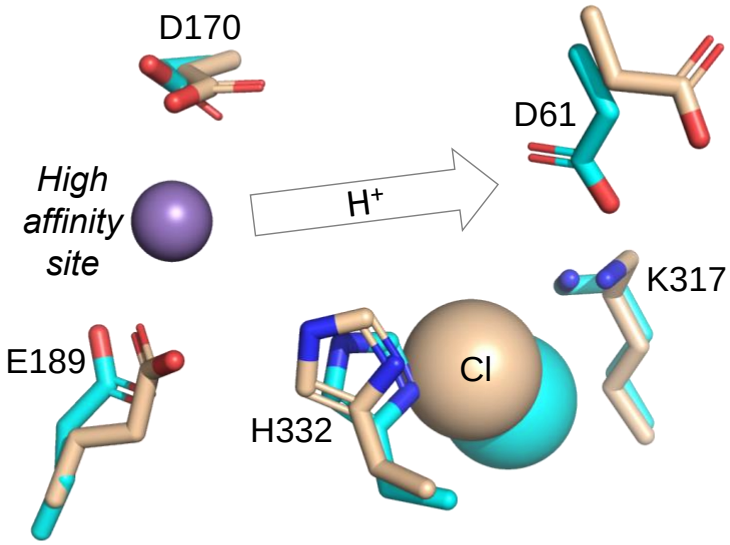


**Figure 5.** Local environment of a proposed $Mn^{2+}$ high-affinity site (HAS). Structures from (Zabret et al. 2021) (7NHO, tan colors) and (Gisriel et al. 2020) (6WJ6, cyan colors) were overlayed in PyMOL. The purple sphere represents the observed ion in 7NHO. We propose that the presence of chloride increases the $pK_a$ of D1-H332 leading to a deprotonation of a $Mn^{2+/3+}$ aqua ligand. In addition, chloride binding leads to an increase in the $pK_a$ of D1-D61 which favors more efficient proton release away from the active site.

Assuming the observed ion in 7NHO (Zabret et al. 2021) is $Mn^{2+}$, the distance to D1-H332 is consistent with a bridging water molecule (Sato et al. 2021). Based on Figure 5, the $pK_a$ of D1-H332 is expected to increase to favor ionic attraction when chloride is bound. In turn, such a histidine would lower the $pK_a$ of the bridging water molecule. Converting a $Mn^{2+}$-aqua ligand to a $Mn^{2+}$-hydroxo ligand will make the $Mn^{3+}/Mn^{2+}$ reduction potential more energetically favorable.

Chloride is expected to also increase the $pK_a$ of D2-K317 to favor ionic attraction. In the absence of chloride, a salt bridge instead forms between D2-K317 and D1-D61 (Pokhrel et al. 2011). With chloride bound, the $pK_a$ of D1-D61 is a higher value making this residue a better Bronstead base. Here, chloride is tuning $pK_a$ values of residues to promote efficient proton release away from the active site.

While $Ca^{2+}$ is required for OEC photo-assembly, the specific role remains unclear. $Mn^{3+}$ can be observed in the absence of $Ca^{2+}$ at high pH (Tyryshkin et al. 2006). However, the absence of $Ca^{2+}$ in intermediate A decreases the rate of electron donation to $Y_Z^{\bullet}$ (Franzén et al. 1985) and increases the back reaction of B to A (Avramov et al. 2020). Dismukes and coworkers proposed a model in which an aqua ligand is deprotonated to form a μ-hydroxo ligand bridging $Mn^{3+}$ and $Ca^{2+}$ (Tyryshkin et al. 2006). Our work here indicates that calcium must be present to accumulate intermediate B ($Mn^{3+}$) at pH 6.0. Where calcium binds in this early stage of photo-assembly remains unclear. However,

our data do provide information on when calcium binds. Because the samples in Figure 3 and Figure S2 were prepared by low temperature illumination where diffusion is limited, $Ca^{2+}$ must bind before or with $Mn^{2+}$. As shown in the lower panel of Figure 3, increasing chloride concentration cannot compensate for the absence of calcium at pH 6.0.

Chloride is an essential PSII cofactor because it tunes the $pK_a$ values of other groups near the OEC. By removing the lumenal extrinsic subunits, we can exaggerate this effect by increasing the $K_d$ of chloride binding. Here, we show that during OEC photo-assembly, the presence of chloride increases the yield of intermediate B, which would otherwise be disfavored at the low pH values of the thylakoid lumen. We propose that B increases in the presence of chloride because the reduction potential of $Mn^{3+}/Mn^{2+}$ is more favorable and protons can be more efficiently shuttled away from the active site. Chloride then makes the rate-determining step of B to C conversion faster by also facilitating deprotonation(s) (Vinyard et al. 2019). These atomic-level mechanistic insights improve our understanding of the assembly of this remarkable active site.

## Acknowledgments

The experimental work was funded the U.S. Department of Energy, Office of Science, Office of Basic Energy Science, Division of Chemical Sciences, Geosciences, and Biosciences, Photosynthetic Systems through Grant DE-SC0020119. B.P.R. was supported by the Herman Frasch Fund for Chemical Research through Grant 822-HF17. Instrumentation support was provided by the Louisiana Board of Regents Support Fund. We thank M. Rita Riggio for technical support.

## References


Avramov, A. P., H. J. Hwang and R. L. Burnap (2020). "The role of $Ca^{2+}$ and protein scaffolding in the formation of nature's water oxidizing complex." Proc. Natl. Acad. Sci. USA 117: 28036. https://doi.org/10.1073/pnas.2011315117

Bao, H. and R. L. Burnap (2016). "Photoactivation: The Light-Driven Assembly of the Water Oxidation Complex of Photosystem II." Front. Plant Sci. 7. https://doi.org/10.3389/fpls.2016.00578

Brinkert, K., S. De Causmaecker, A. Krieger-Liszkay, A. Fantuzzi and A. W. Rutherford (2016). "Bicarbonate-induced redox tuning in Photosystem II for regulation and protection." Proc. Natl. Acad. Sci. USA 113: 12144. https://doi.org/10.1073/pnas.1608862113

Burnap, R. L., M. Qian and C. Pierce (1996). "The Manganese-Stabilizing Protein of Photosystem II Modifies the in Vivo Deactivation and Photoactivation Kinetics of the $H_2O$ Oxidation Complex in Synechocystis sp. PCC6803." Biochemistry 35: 874-882. https://doi.org/10.1021/bi951964j

Campbell, K. A., D. A. Force, P. J. Nixon, F. Dole, B. A. Diner and R. D. Britt (2000). "Dual-Mode EPR Detects the Initial Intermediate in Photoassembly of the Photosystem II Mn Cluster: The Influence of Amino Acid Residue 170 of the D1 Polypeptide on Mn Coordination." J. Am. Chem. Soc. 122: 3754-3761. https://doi.org/10.1021/ja000142t

Chen, C., J. Kazimir and G. M. Cheniae (1995). "Calcium Modulates the Photo-assembly of Photosystem II $(Mn)_4$-Clusters by Preventing Ligation of Nonfunctional High-Valency States of Manganese." Biochemistry 34: 13511-13526. https://doi.org/10.1021/bi00041a031

Dasgupta, J., G. M. Ananyev and G. C. Dismukes (2008). "Photoassembly of the water-oxidizing complex in photosystem II." Coord. Chem. Rev. 252: 347-360. https://doi.org/https://doi.org/10.1016/j.ccr.2007.08.022

Dasgupta, J., A. M. Tyryshkin, S. V. Baranov and G. C. Dismukes (2009). "Bicarbonate Coordinates to $Mn^{3+}$ during Photo-Assembly of the Catalytic $Mn_4Ca$ Core of Photosynthetic Water Oxidation: EPR Characterization." Appl. Magn. Reson. 37: 137. https://doi.org/10.1007/s00723-009-0053-z

Franzén, L.-G., Ö. Hansson and L.-E. Andréasson (1985). "The roles of the extrinsic subunits in Photosystem II as revealed by EPR." Biochim. Biophys. Acta - Bioenerg. 808: 171-179. https://doi.org/https://doi.org/10.1016/0005-2728(85)90040-4

Gisriel, C. J., K. Zhou, H.-L. Huang, R. J. Debus, Y. Xiong and G. W. Brudvig (2020). "Cryo-EM Structure of Monomeric Photosystem II from Synechocystis sp. PCC 6803 Lacking the Water-Oxidation Complex." Joule 4: 2131-2148. https://doi.org/https://doi.org/10.1016/j.joule.2020.07.016

Jensen, C. M. and D. W. Lee (2000). "Dry-Ice Bath Based on Ethylene Glycol Mixtures." J. Chem. Ed. 77: 629. https://doi.org/10.1021/ed077p629

Kramer, D. M., C. A. Sacksteder and J. A. Cruz (1999). "How acidic is the lumen?" Photosyn. Res. 60: 151-163. https://doi.org/10.1023/A:1006212014787

Miller, A. F. and G. W. Brudvig (1989). "Manganese and calcium requirements for reconstitution of oxygen-evolution activity in manganese-depleted photosystem II membranes." Biochemistry 28: 8181-8190. https://doi.org/10.1021/bi00446a033

Miller, A. F. and G. W. Brudvig (1990). "Electron-transfer events leading to reconstitution of oxygen-evolution activity in manganese-depleted photosystem II membranes." Biochemistry 29: 1385-1392. https://doi.org/10.1021/bi00458a007

Miyao, M. and Y. Inoue (1991). "Enhancement by chloride ions of photoactivation of oxygen evolution in manganese-depleted photosystem II membranes." Biochemistry 30: 5379-5387. https://doi.org/10.1021/bi00236a008

Pokhrel, R., I. L. McConnell and G. W. Brudvig (2011). "Chloride Regulation of Enzyme Turnover: Application to the Role of Chloride in Photosystem II." Biochemistry 50: 2725-2734. https://doi.org/10.1021/bi2000388

Radmer, R. and G. M. Cheniae (1971). "Photoactivation of the manganese catalyst of $O_2$ evolution. II. A two-quantum mechanism." Biochim. Biophys. Acta - Bioenerg. 253: 182-186. https://doi.org/https://doi.org/10.1016/0005-2728(71)90243-X

Roose, J. L. and H. B. Pakrasi (2008). "The Psb27 Protein Facilitates Manganese Cluster Assembly in Photosystem II." J. Biol. Chem. 283: 4044-4050. https://doi.org/10.1074/jbc.M708960200

Sato, A., Y. Nakano, S. Nakamura and T. Noguchi (2021). "Rapid-Scan Time-Resolved ATR-FTIR Study on the Photoassembly of the Water-Oxidizing $Mn_4CaO_5$ Cluster in Photosystem II." J. Phys. Chem. B 125: 4031-4045. https://doi.org/10.1021/acs.jpcb.1c01624

Shen, J.-R. (2015). "The Structure of Photosystem II and the Mechanism of Water Oxidation in Photosynthesis." Annu. Rev. Plant Biol. 66: 23-48. https://doi.org/10.1146/annurev-arplant-050312-120129

Stoll, S. and A. Schweiger (2006). "EasySpin, a comprehensive software package for spectral simulation and analysis in EPR." J. Magn. Reson. 178: 42-55. https://doi.org/https://doi.org/10.1016/j.jmr.2005.08.013

Tao, L., T. A. Stich, A. V. Soldatova, B. M. Tebo, T. G. Spiro, W. H. Casey and R. D. Britt (2018). "Mn(III) species formed by the multi-copper oxidase MnxG investigated by electron paramagnetic resonance spectroscopy." J. Biol. Inorg. Chem. 23: 1093-1104. https://doi.org/10.1007/s00775-018-1587-z

Tyryshkin, A. M., R. K. Watt, S. V. Baranov, J. Dasgupta, M. P. Hendrich and G. C. Dismukes (2006). "Spectroscopic Evidence for $Ca^{2+}$ Involvement in the Assembly of the $Mn_4Ca$ Cluster in the Photosynthetic Water-Oxidizing Complex." Biochemistry 45: 12876-12889. https://doi.org/10.1021/bi061495t

Umena, Y., K. Kawakami, J.-R. Shen and N. Kamiya (2011). "Crystal structure of oxygen-evolving photosystem II at a resolution of 1.9 Å." Nature 473: 55-60. https://doi.org/10.1038/nature09913

Vinyard, D. J., S. L. Badshah, M. R. Riggio, D. Kaur, A. R. Fanguy and M. R. Gunner (2019). "Photosystem II oxygen-evolving complex photoassembly displays an inverse H/D solvent isotope effect under chloride-limiting conditions." Proc. Natl. Acad. Sci. USA 116: 18917. https://doi.org/10.1073/pnas.1910231116

Vinyard, D. J. and G. W. Brudvig (2017). "Progress Toward a Molecular Mechanism of Water Oxidation in Photosystem II." Annu. Rev. Phys. Chem. 68: 101-116. https://doi.org/10.1146/annurev-physchem-052516-044820

Zabret, J., S. Bohn, S. K. Schuller, O. Arnolds, M. Möller, J. Meier-Credo, P. Liauw, A. Chan, E. Tajkhorshid, J. D. Langer, R. Stoll, A. Krieger-Liszkay, B. D. Engel, T. Rudack, J. M. Schuller and M. M. Nowaczyk (2021). "Structural insights into photosystem II assembly." Nature Plants 7: 524-538. https://doi.org/10.1038/s41477-021-00895-0